

University of Arkansas, Fayetteville

ScholarWorks@UARK

Mechanical Engineering Undergraduate Honors
Theses

Mechanical Engineering

5-2021

Mathematical Modeling of a Two Wheeled Robotic Base

Kathryn Remell

Follow this and additional works at: <https://scholarworks.uark.edu/meeguht>



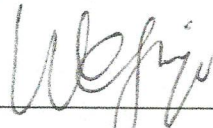
Part of the [Acoustics, Dynamics, and Controls Commons](#), and the [Applied Mechanics Commons](#)

Citation

Remell, K. (2021). Mathematical Modeling of a Two Wheeled Robotic Base. *Mechanical Engineering Undergraduate Honors Theses* Retrieved from <https://scholarworks.uark.edu/meeguht/96>

This Thesis is brought to you for free and open access by the Mechanical Engineering at ScholarWorks@UARK. It has been accepted for inclusion in Mechanical Engineering Undergraduate Honors Theses by an authorized administrator of ScholarWorks@UARK. For more information, please contact ccmiddle@uark.edu.

This thesis has been approved by the Mechanical Engineering Department for submittal to the College of Engineering and the Honors College at the University of Arkansas.

 4/28/2020 (Signature and Date)
MEEG Honors Advisor

Adam Huang Digitally signed by Adam Huang
Date: 2020.04.28 10:53:45
-05'00' (Signature and Date)

Honors Committee Member

 4/28/2020 (Signature and Date)
Departmental Honors Coordinator or Department Head

NOTE: This form must be signed and inserted into the final PDF of the honors thesis before submittal.

Mathematical Modeling of a Two Wheeled Robotic Base

An Honors Thesis submitted in partial fulfillment of the requirements
for the Honors Program in Mechanical Engineering

by

Kathryn Remell

Tarrant County College

Associates of Arts, 2004

Spring 2020

University of Arkansas

Abstract

This thesis presents the concept of using a two wheeled robot on the moon and briefly explores the requirements for successful long term operation in a lunar environment. The mathematical model for the motion of a robot with two fixed wheels on a differential drive with in a global reference frame. The robot is assumed to be balancing a platform so the mathematical model to balance the platform with wheel motors is also developed and briefly evaluated.

Acknowledgements

Dr. Wejinya for patiently working with me while I developed and explored several thesis concepts and also for consistently challenging me to expand my skills while helping me learn how to gauge the possible. I have grown as an engineer and person because of his time and assistance as my honor's advisor.

Dr. Haung for demonstrating enthusiasm and excitement about every subject I have had the good fortune to learn from him and for being a member of my thesis committee.

Table of Contents

Abstract.....	2
Acknowledgements.....	3
Table of Contents.....	4
Table of Figures.....	6
1. Introduction.....	7
Objective.....	7
Related Work.....	7
Design Considerations.....	8
Stability.....	8
The Lunar Environment.....	9
Launching.....	9
2. Nomenclature.....	11
Variables.....	11
Subscripts.....	12
Superscripts.....	12
Greek Variables.....	13
Symbols.....	13
3. Mathematical Model of a Generic Two Wheeled Robot.....	14
Kinematic Model of Motion with Constraints.....	14
Kinematic Model of Motion.....	14
Constraints on Motion.....	20
Pendulum Kinematic Model.....	23
Kinematic Equations.....	24
Dynamic Equations.....	26
Transfer Function and Matrix Equations.....	27
4. Model Analysis.....	31
Testing Mathematical Model in Matlab.....	31
Simulation Results.....	31
Error Analysis.....	33
5. Conclusions & Future Work.....	34
Conclusions.....	34
Future Work.....	34

Controls Development and Implementation.....	34
Physical Design and Construction.....	35
6. References	36
7. Appendix.....	38
Appendix A: Values Tested	38
Appendix B: Matlab Code	38
Appendix C: Transfer Function Output:	40
Test 1	40
Test 2	41
Test 3	42
Test 4	43
Test 5	44
Test 6	45
Test 7	46

Table of Figures

Figure 1: Differential Drive Robot Reference Frame in a Global Reference Frame.	15
Figure 2: Surface arc on the wheel as it turns is equal to the distance traveled by the wheel [14].	16
Figure 3: Relationship between tangential velocity and angular momentum.....	16
Figure 4: Distance between wheels and the robot's center point.	17
Figure 5: Instantiation Center of Rotation (ICR) for wheel 2 when wheel 1 is held stationary. ...	18
Figure 6: Top view of left front wheel of four wheeled differential drive robot with fixed wheels and the center point located in the center of the robot [13].	20
Figure 7: Face view of wheel 1 with motion in the +XR direction as shown in Figure 4.	21
Figure 8: Face view of wheel 2 with motion in the +XR direction as shown in Figure 4.	21
Figure 9: Platform's Reference Frame.....	23
Figure 10: Robot's Reference Frame	23
Figure 11: Wheel Rotation to Platform Angle (Angle from Vertical)	23
Figure 12: Free Body Diagram and Effective Force Diagram of the Robot Base	24
Figure 13: Free Body Diagram and Effective Force Diagram of the Robot Platform	25
Figure 14: Free Body Diagram and Effective Force Diagram of the Platform Showing Force Components	25
Figure 15: Diagram of Moment Arms of Forces Acting on the Platform	25
Figure 16: Step and Impulse of the Angle from Vertical to Motor Torque (Eq. 74).....	32
Figure 17: Step and Impulse Response of Wheel Angular Acceleration to Motor Torque (Eq. 76)	32
Figure 18: Test 1 Step and Impulse Response.....	40
Figure 19: Test 2 Step and Impulse Response.....	41
Figure 20: Test 3 Step and Impulse Response.....	42
Figure 21: Test 4 Step and Impulse Response.....	43
Figure 22: Test 5 Step and Impulse Response.....	44
Figure 23: Test 6 Step and Impulse Response.....	45
Figure 24: Test 7 Step and Impulse Response.....	46

1. Introduction

Objective

The goal of this thesis is to develop the mathematical model for a mobile robotic platform suitable for use as an effector base in a lunar environment. Precise control of the base robot is required to allow the mounted tool to perform precise actions. Since the functional environment is lunar, the robotic base must also be able to withstand temperatures from 392.3K (246.47°F or 119.15°C) [1] to 50K (-369.67°F or -223.15°C) [2]. It must also be able to gather and store enough power to function during the 327.84 hour (13.66 earth days) lunar night [3] and be robust enough to withstand launch and navigation over lunar soil. In addition, the robot should be small and lightweight enough to be launched from earth using existing low cost launch platforms.

Related Work

A number of two wheeled robots have been designed with similar physical characteristics and several different control methods have been investigated and proven to be successful at stabilizing and controlling a two wheeled pendulum base. These methods include Sliding Mode [4] [5], PID [6], Linear Quadratic Gaussian [7] [6], and Evolutionary Fuzzy Control through “an adaptive fusion of continuous ant colony optimization and particle swarm optimization” [8]. All of the control methods provide stability and basic motion and several authors have begun expanding capabilities into navigation and object detection [9].

While all of the control systems have been tested through software simulation, most of them have not been subjected to real world evaluation. Those that have been tested, demonstrated several unique capabilities and functional areas where the two wheeled design excels. Dynamic stabilization, a strength of two wheeled robots, has been demonstrated to lead to robots that are better at handling heavy objects with a smaller support base [10] than a robot dependent on static stability, such as a stationary arm or a three or more wheeled robot. This leads to the conclusion that a two wheeled robot is more versatile and is a robust mobile design

capable of handling larger shifts in the center of gravity [7]. This capability makes it easier to handle unexpected impulse inputs when navigating and able to support a wider range of motion in end-effectors than four wheeled robots of the same size. In addition, two wheeled systems are highly maneuverable which makes them capable of performing on uneven surfaces in confined spaces [6].

The greatest commonality between the articles surveyed was the focus on design and control for terrestrial use and, for those physically constructed robots, task oriented design [4] [7] [8] [9] [10]. This thesis investigates the design of a modular system capable of supporting a variety of effectors and designed to function outside of the usual terrestrial environment. Such investigation has become pertinent due to NASA's increased interest in building permanent habitation on the moon and pursuing further research [3] facilitated by such a location. This design could also be instrumental in building habitations on Mars, likely with minor modifications to physical components, mining asteroids, and aiding astronauts on any mission with sufficient gravity to allow the robotic base to operate.

Design Considerations

Stability

The goal of this thesis is to investigate the design and control for a two wheeled robotic platform which can be used as a mobile base for a variety of instruments and effectors, such as a robotic arm or a 3D printing nozzle. To meet this goal attention should be given to the physical design of the platform to facilitate convenient attachment with a tool specific adapter and to the systems control to provide a stable base both during movement and when stationary. Both of these are affected by the geometry of the robot components, so the first step should be establishing how the geometry effects the robot's stability.

The Lunar Environment

While such a robot has a wide range of applications, designing for the lunar environment will meet the most immediate need [3]. The temperature on the moon reaches 392.3K (246.47°F or 119.15°C) at the equator [1] and can drop down to 50K (-369.67°F or -223.15°C) [2] at the north pole. NASA's current mission focus is on the South Pole [3], which experiences temperatures only about 11K higher, making design for the temperature extremes vital.

The cheapest long term solution to power generation may be solar since it is likely to reduce the complexity of the system over the alternatives employed by other extraterrestrial vehicles. However, solar does introduce the problem of power storage at night. One lunar revolution is 27.32 days [1] which means that the robot must be able to store sufficient power to either be functional during the 13.66 days of night or maintain its core systems while dormant. Sufficient power storage would also allow the robot to function inside permanently dark craters and underground should the need arise.

Launching

Even with recent advancements launching something into space is expensive based on SpaceX's Falcon 9, the cheapest launch platform, \$63 million cost to launch 22,800kg [11]. For smaller satellites and pocketbooks Spaceflight, a launch company providing space on rocket launches for as little as \$140,000/kg for a 10cm x 22.63cm x 34.05cm or less object that weights up to 10kg [12]. While the price per kilogram is higher than SpaceX's \$2,720/kg, the total price tag for launch is more reasonable for an unmanned research and development lunar mission. Designing a robot base that would fit inside the given dimensions along with an instrument provides more opportunity for a quick lunar delivery on regularly scheduled launches as well as scalability in the future. Therefore, the robot prototype should be able to fit within an 8cm x 20cm x 20cm cube with a goal maximum weight of 2.5kg. This would allow room for a system propel the robot to the moon from the rocket's release point as well as an attached tool or instrument.

2. Nomenclature

Variables

- \vec{a} Acceleration
- B A generic non-square matrix
- C Center
- d Vertical distance from the point of rotation to the platform's center of gravity (m)
- F Force
- \vec{g} Gravity ($\frac{m}{s^2}$)
- I Moment of Inertia ($kg\ m^2$)
- J Matrix of fixed wheel rolling without slipping constraints
- K Diagonal matrix of each wheel's radii
- l Distance from the center of the robot's reference frame to the center of the wheels
- m Mass (kg)
- M Moments
- N Normal Force (N)
- o Horizontal distance from point of rotation to the platform's center of gravity (cm)
- q Simplification equation
- R Rotational Matrix
- r Radius of the wheel (m)
- S Matrix of orthogonal sliding constraints for all wheels
- s Transfer Function Variable
- t Time (s)
- T Period of a full revolution
- v Tangential (linear) velocity

- X x-axis (forms a horizontal plane parallel to the ground with the y-axis)
- x Position along the x-axis, Arc length on wheel
- Y y-axis (forms a horizontal plane parallel to the ground with the x-axis)
- y Position along the y-axis
- Z z-axis (vertical axis perpendicular to the ground)
- z Position along the z-axis

Subscripts

- 1, 2, ... 1st, 2nd, etc. of the attached variable
- C Center
- COR Center of Rotation
- f Friction
- \vec{g} Gravity
- G Global reference frame
- n Normal
- P Platform reference frame
- R Robot base's reference frame
- t Tangential
- w Wheel
- X x-axis (forms a horizontal plane parallel to the ground with the y-axis)
- Z z-axis (vertical axis perpendicular to the ground)

Superscripts

- -1 Inverse of attached variable
- $+$ The pseudoinverse of a non-square matrix
- H Transpose of a Matrix
- n A number (1, 2, etc.)

- 2, 3, ... Raised to the Power of 2, 3, etc.

Greek Variables

- α Angular acceleration
- β Angle between the robot's reference frame and the wheel plane's normal
- δ Angle between wheel position and robot's reference frame
- γ Wheel angle of rotation
- Γ Laplace transformation of the function γ
- η Angle between the robot's z-axis and the platform's z-axis (Angle from Vertical)
- H Laplace transformation of the function η
- θ Angle of orientation between reference frames
- ξ Position Matrix
- τ Torque
- Ω Matrix composed of each wheel's angular velocity
- ω Angular velocity (rad/s)

Symbols

- $+\uparrow, +\rightarrow$ Positive direction of forces being summed
- $+\cup$ Clockwise, Positive direction of moments being summed
- Δ Delta, Change in (Derivative of) the variable it precedes
- \cdot First derivative with respect to time, Velocity
- $\ddot{}$ Second derivative with respect to time, Acceleration
- \mathcal{L} Laplace Transformation
- Σ Sum of following variable
- $\vec{}$ Vector, Variable has both direction and magnitude

3. Mathematical Model of a Generic Two Wheeled Robot

Physical parameters such as the wheel diameter, the distance between the wheels, and the height of the center of gravity have a strong influence on the controllability of a robot and adjusting those dimensions can have a significant effect on the stability of the robotic platform. Therefore, development of the two wheeled robot must be started with the mathematical model for a generic two wheeled robot. Such a model will allow the various geometric parameters to be tested in a software simulation to inform the physical design of the robot.

Two major components of motion are navigation and balance. The mathematical model required for navigation is the kinematic model of a two wheeled robot. The mathematical model for balance is an inverted pendulum. The full mathematical model combines these two equations.

Kinematic Model of Motion with Constraints

The kinematic model of motion for a two wheeled robot with fixed wheels and a differential drive was determined by first considering the motion of the robot and then applying appropriate constraints, rolling without slipping and no movement normal to the wheel plane, to the wheels.

Kinematic Model of Motion

The kinematic model of a two wheeled robot with fixed wheels was found by considering the motion of the wheels as described in [13]. First, the robots location relative to its environment was described by assigning the robot and its environment a reference frame and defining the robots location and orientation relative to the global reference frame. Since both reference frames can have an arbitrarily defined origin, the robot's center of mass was selected for the origin of the robot's reference frame for simplification purposes. The robot's center of mass was assumed to be positioned equidistant between the wheels and its height irrelevant for navigation.

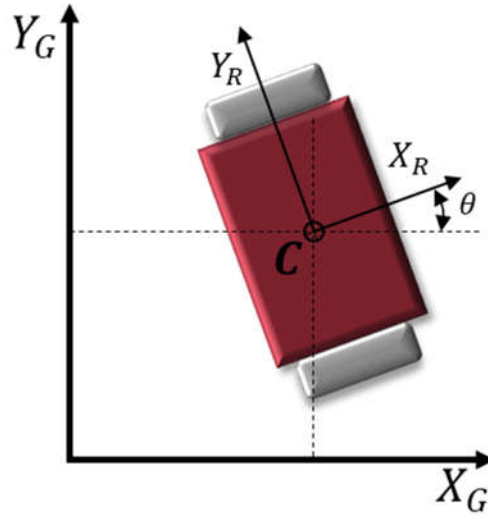


Figure 1: Differential Drive Robot Reference Frame in a Global Reference Frame.

Three generalized coordinates were required to specify the robot's location and orientation relative to the environment. Referring to Figure 1 the coordinates (x, y) were chosen to specify the robot's location and the angle θ was chosen to indicate the robot's angle of orientation relative to the global reference frame. These three coordinates are combined into one vector, Eq. 1, to facilitate translation from one reference frame to the other.

$$\xi_G = \begin{bmatrix} x \\ y \\ \theta \end{bmatrix} \quad \text{Eq. 1}$$

The orthogonal rotational matrix shown in Eq. 2 was used to map the robot's motion to the global reference frame.

$$R(\theta) = \begin{bmatrix} \cos\theta & \sin\theta & 0 \\ -\sin\theta & \cos\theta & 0 \\ 0 & 0 & 1 \end{bmatrix} \quad \text{Eq. 2}$$

To specify the robot's motion (velocity) in terms of the global reference frame the derivative of the position vector was taken, as shown in Eq. 3. Then, it was multiplied by the rotational matrix to form Eq. 4 which specified the robot's motion in the robot's reference frame.

$$\dot{\xi} = \begin{bmatrix} \dot{x} \\ \dot{y} \\ \dot{\theta} \end{bmatrix} \quad \text{Eq. 3}$$

$$\dot{\xi}_R = R(\theta)\dot{\xi}_G \quad \text{Eq. 4}$$

The robot's motion in the global reference frame was defined by premultiplying the inverse of the rotational matrix with the robot's velocity to get Eq. 5.

$$\dot{\xi}_G = R^{-1}(\theta)\dot{\xi}_R \quad \text{Eq. 5}$$

To define the robot's motion, the physical components of the robot that produce that motion were considered. The radius of the robot's wheels determines the velocity and distance traveled. As the wheel's turn, the point of contact between the wheel and the ground rotates along the wheel's surface. The arc length between the points starting position on the wheel and its final position equal the distance traveled by the wheel's center of rotation, as shown in Figure 2. Mathematically, the arc length equals the radius of the wheel times the angle of rotation, so the distance traveled is defined by Eq. 6

$$x(t) = r\gamma(t) \quad \text{Eq. 6}$$

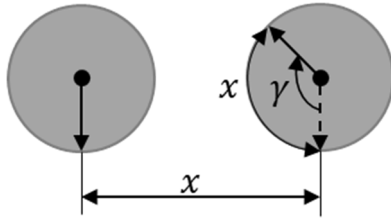


Figure 2: Surface arc on the wheel as it turns is equal to the distance traveled by the wheel [14].

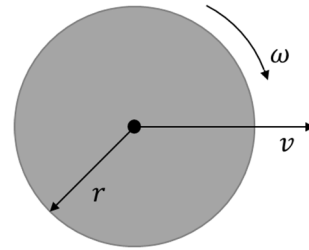


Figure 3: Relationship between tangential velocity and angular momentum.

As represented in Figure 3, the tangential velocity of the center of rotation is equal to the radius of the wheel times the angular velocity of the wheel.

$$v = \dot{x} = r\omega \quad \text{Eq. 7}$$

The angular velocity is the first derivative of the wheel's angle of rotation [14],

$$\omega = \frac{d\gamma(t)}{dt} = \dot{\gamma} \quad \text{Eq. 8}$$

A full revolution during a full period of rotation is 2π , see Eq. 9.

$$\omega = \frac{2\pi}{T} \quad \text{Eq. 9}$$

This meant that rotation beyond a full revolution must be multiplied by the number of rotations to represent the distance travelled. To simplify evaluation, the model was developed based on less than full wheel rotation with later implementation to include the multiple.

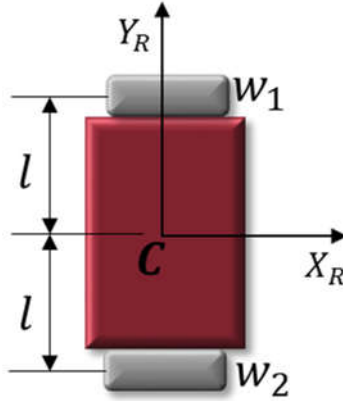


Figure 4: Distance between wheels and the robot's center point.

The last physical parameter that affected the robot's motion was the distance between the wheels and the center of mass of the robot, C , shown in Figure 4, which was defined to be l . This allowed the motion in the global reference frame to be defined as shown in Eq. 10, where θ was included to determine the angle of travel from the global reference frame.

$$\dot{\xi}_G = f(l, r, \theta, \omega_1, \omega_2) \quad \text{Eq. 10}$$

Recall Eq. 3 where \dot{x} represented the velocity of the center point, C , along the x-axis, \dot{y} represented the velocity along the y-axis, and $\dot{\theta}$ represented the angular difference between the global and robot's reference frames. The wheel plane was defined as a plane through the center of the wheel parallel to the x-axis shown in Figure 4. Therefore, the velocity in the y-axis direction must be zero since the robot's motion is constrained to prevent movement normal to the wheel plane, so $\dot{y} = 0$.

The velocity in the x-axis direction \dot{x} , was defined to be the sum of the velocity of each wheel as experienced at the center. To determine \dot{x} one wheel was held still and the other rotated,

which demonstrated that the rotating wheel's Instantaneous Center of Rotation was about the stationary wheel, as shown in Figure 5. Since C was located halfway between the two wheels, at half the rotation radius, it only experienced half of the velocity generated by the rotating wheel.

Therefore, the component of the velocity from each wheel is $\frac{1}{2}r\omega$, so

$$\dot{x} = \frac{1}{2}r(\omega_1 + \omega_2). \quad \text{Eq. 11}$$

Eq. 11 was verified by considering the case when wheel one spun in one direction and the other wheel spun in the opposite direction. Assuming both wheels had the same speed, then the differential drive robot should spin in circles and the velocity in the $+X_R$ direction seen by C should be zero. Plugging the assumption about direction and magnitude of velocity into Eq. 11 results in

$$\dot{x} = \frac{1}{2}r(\omega_1 + \omega_2) = \frac{1}{2}r(\omega - \omega) = 0 \quad \text{Eq. 12}$$

as expected.

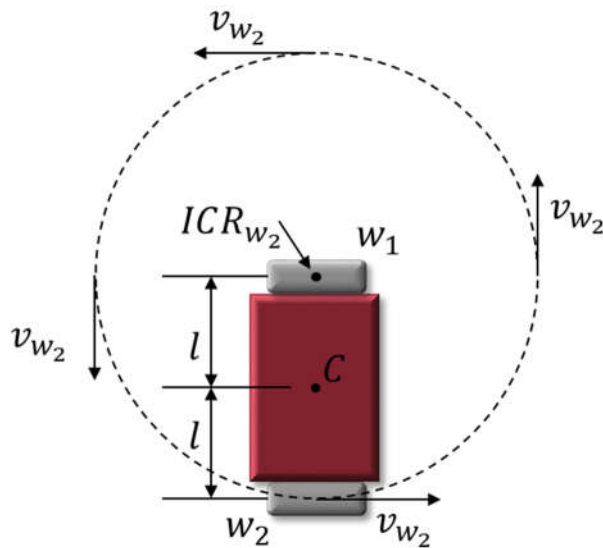


Figure 5: Instantiation Center of Rotation (ICR) for wheel 2 when wheel 1 is held stationary.

Since w_2 moved along an arc about w_1 in a counter clockwise direction, $\dot{\theta}$, the rotational velocity at C , can be computed by treating the robot body as a rotating disk with radius $2l$, shown

in Figure 5, and the rotating wheel (w_2) at a point on the edge. The rotational component of the disk was defined using Eq. 6, Eq. 7, and Eq. 8 to be

$$\omega_{disk} = \dot{\gamma} = \frac{\dot{x}}{r_{disk}} = \frac{v_{disk}}{r_{disk}} \quad \text{Eq. 13}$$

The tangential velocity of the center of the disk was the tangential velocity of w_2 , so

$$v_{disk} = v_{w_2} = (r\omega)_{w_2} \quad \text{Eq. 14}$$

which allowed Eq. 13 to be rewritten in terms of the wheel's parameters and the counter clockwise direction of rotation:

$$\omega_{disk} = -\frac{(r\omega)_{w_2}}{2l} \quad \text{Eq. 15}$$

Eq. 15 represented the angle of the robot's reference frame from the global reference frame due to w_2 . The angle due to w_1 was found the same way

$$\omega_{disk} = \frac{(r\omega)_{w_1}}{2l} \quad \text{Eq. 16}$$

since spin in the $+X_R$ direction resulted in a clockwise rotation of the disk. Subsequently, the two were summed to determine the total change of the orientation between reference frames, resulting in

$$\dot{\theta} = \frac{r}{2l}(\omega_1 - \omega_2) \quad \text{Eq. 17}$$

Therefore, the robot's motion was described by

$$\dot{\xi}_R = \begin{bmatrix} \frac{r}{2}(\omega_1 + \omega_2) \\ 0 \\ \frac{r}{2l}(\omega_1 - \omega_2) \end{bmatrix}. \quad \text{Eq. 18}$$

Taking the inverse of the rotational matrix (Eq. 2) and plugging the result and Eq. 18 into Eq. 5 resulted in the description of the robot's motion relative to the global reference frame shown by Eq. 19.

$$\dot{\xi}_G = R^{-1}(\theta)\dot{\xi}_R = \begin{bmatrix} \cos\theta & -\sin\theta & 0 \\ \sin\theta & \cos\theta & 0 \\ 0 & 0 & 1 \end{bmatrix} \begin{bmatrix} \frac{r}{2}(\omega_1 + \omega_2) \\ 0 \\ \frac{r}{2l}(\omega_1 - \omega_2) \end{bmatrix} \quad \text{Eq. 19}$$

Constraints on Motion

As described, for a wheel to move along its rim across a horizontal surface two constraints are applied, the wheel must roll without slipping and the wheel cannot move normal to the wheel plane. Due to internal wheel degrees of freedom, only fixed and steerable wheels affect the kinematics of motion [13]. Based on the survey of literature, fixed wheels provide the greatest maneuverability for a two wheeled vehicle, so constraint equations were developed for a fixed wheeled robots.

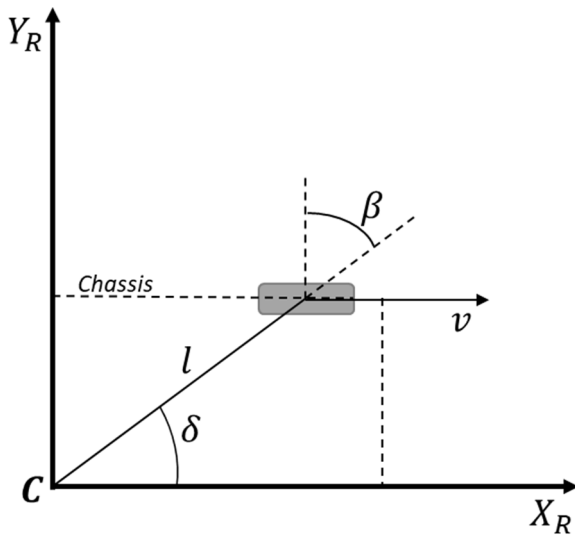


Figure 6: Top view of left front wheel of four wheeled differential drive robot with fixed wheels and the center point located in the center of the robot [13].

The wheel's orientation relative to the center and the robots' coordinate frame is shown in Figure 6. The position of the wheel relative to the center was defined to be a distance l from the center at an angle δ , which combine in polar coordinates. The angle between the wheel plane and the chassis, defined as β , is constant for a fixed wheel. As previously described the rotation of the wheel about its horizontal axis, see Figure 2, given by Eq. 6, is a function of time:

$$x(t) = \gamma(t)r \quad \text{Eq. 20}$$

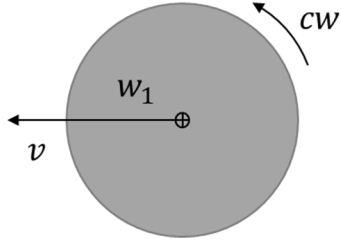


Figure 7: Face view of wheel 1 with motion in the $+X_R$ direction as shown in Figure 4.

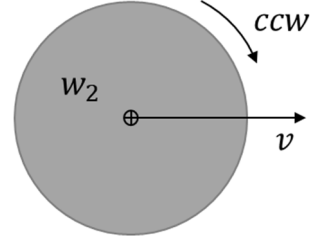


Figure 8: Face view of wheel 2 with motion in the $+X_R$ direction as shown in Figure 4.

To develop the constraint equations the motion of each wheel of the robot was considered with the axle facing away as shown in Figure 7 and Figure 8. For the center of the wheel to move in the positive X_R direction wheel one, which is on the positive Y_R axis, must spin clockwise, see Figure 7, and wheel two, which is on the negative Y_R axis, must spin counter clockwise, see Figure 8. Therefore, the angle between C and the center of wheel one, δ in Figure 6, is $\pi/2$ and the angle between the normal to the wheel plane and the center point, β , is zero, and for wheel two, $\delta = -\pi/2$ and $\beta = -\pi$.

A fixed wheel's motion is limited to strictly along the wheel plane and rotation about the point of contact with the ground [13]. To ensure that all motion along the wheel plane is accompanied by an equivalent amount of wheel spin (see Figure 2) let

$$[\sin(\delta + \beta) \quad -\cos(\delta + \beta) \quad -l\cos\beta] R(\theta)\dot{\xi}_G = r\omega(t), \quad \text{Eq. 21}$$

where $\omega(t)$ is defined by Eq. 8. The three components of the vector on the left in Eq. 21 mapped the contribution of \dot{x} , \dot{y} , and $\dot{\theta}$, transformed from the global reference frame by the term $R(\theta)\dot{\xi}_G$, into motion along the wheel plane in the robot's reference frame. The term on the right represented the rotation of the wheel, which means that Eq. 21 represented constrained motion along the wheel plane such that all motion must be due to wheel rotation. In addition to rolling without slipping the wheel must not slide or move orthogonal to the wheel plane, so

$$[\cos(\delta + \beta) \quad \sin(\delta + \beta) \quad l\sin\beta] R(\theta)\dot{\xi}_G = 0 \quad \text{Eq. 22}$$

must hold true. To make calculation easier the constraints for each wheel were combined so that

$$J = \begin{bmatrix} \sin(\delta_1 + \beta_1) & -\cos(\delta_1 + \beta_1) & -l\cos\beta_1 \\ \sin(\delta_2 + \beta_2) & -\cos(\delta_2 + \beta_2) & -l\cos\beta_2 \end{bmatrix} \quad \text{Eq. 23}$$

represented the rolling without slipping constraint for all wheels, and

$$S = \begin{bmatrix} \cos(\delta_1 + \beta_2) & \sin(\delta_1 + \beta_2) & -l\sin\beta_1 \\ \cos(\delta_2 + \beta_2) & \sin(\delta_2 + \beta_2) & -l\sin\beta_2 \end{bmatrix} \quad \text{Eq. 24}$$

represented the constraint on movement orthogonal to the wheel plane for all wheels. Applying these to the robot's reference frame resulted in

$$JR(\theta)\dot{\xi}_G = K\Omega \quad \text{Eq. 25}$$

$$SR(\theta)\dot{\xi}_G = 0 \quad \text{Eq. 26}$$

$$K = \begin{bmatrix} r_1 & 0 \\ 0 & r_2 \end{bmatrix} \quad \text{Eq. 27}$$

$$\Omega = \begin{bmatrix} \omega_1 \\ \omega_2 \end{bmatrix}. \quad \text{Eq. 28}$$

Eq. 25 and Eq. 26 where the constraint equation in the global reference frame where Eq. 27 was the matrix of wheel radii and Eq. 28 was the matrix of wheel angular velocities.

To represent the robot's motion in the global reference frame compute

$$\dot{\xi}_G = R^{-1}(\theta)J^{-1}K\Omega \quad \text{Eq. 29}$$

which required finding the inverse of the non square matrix J , Eq. 23. This was accomplished by finding the pseudoinverse as described in [15], by

$$B^+ = (B^H B)^{-1} B^H \quad \text{Eq. 30}$$

where B is the non square matrix and B^H is the transpose of B .

The similarity between Eq. 25 and Eq. 19 was noted, which implied that the pseudoinverse of Eq. 23 is Eq. 18. Since Eq. 18 described the motion of the robot in the robot's reference frame, this equivalency held. Therefore, Eq. 19 represented the kinematic model for the motion of a two wheeled differential drive robot with fixed wheels, while Eq. 26 provided a way to evaluate the maneuverability of the system and its workspace.

Pendulum Kinematic Model

A two-wheeled robot is inherently unstable due to the platform supports being inline, which allows the 'front' and 'back' of the platform to oscillate. To achieve a stable base for any tools mounted to the two-wheeled robot the platform must be balanced to within an acceptable degree of vertical defined by η . Balance is achieved and maintained by applying a force to the base of the platform by moving the wheels. With reference to [16] the kinematic equations will be determined, the dynamic equations developed, and then the result will be used to complete the balance equations in terms of the wheel rotation γ and the platforms angle from vertical η .

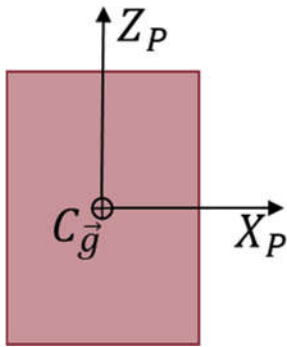


Figure 9: Platform's Reference Frame

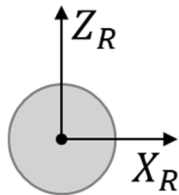


Figure 10: Robot's Reference Frame

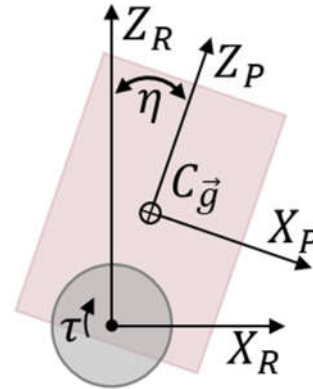


Figure 11: Wheel Rotation to Platform Angle (Angle from Vertical)

Figure 11 illustrates the desired input (motor torque) and output (angle from vertical) variables. The platform's reference frame was defined as shown in Figure 9 and the robot's reference frame as shown in Figure 10, so when the platform is balanced the two z-axes should be collinear. Therefore, the angle η should be as close to zero as possible, within an acceptable margin of error. The relationship between torque (τ) and the angle to vertical was determined by starting with a Free Body Diagram of the wheel base and another of the platform to define the kinematic equations for both, followed by developing the dynamic equations, and finally defining the transfer equations.

Kinematic Equations

Base

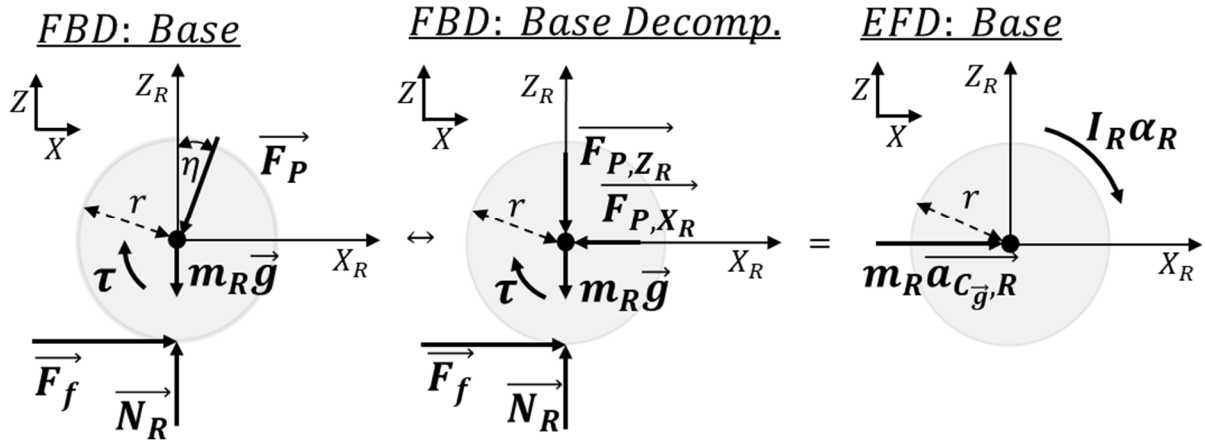


Figure 12: Free Body Diagram and Effective Force Diagram of the Robot Base

For the robot base, the forces in the Z direction, the X direction, and the moments about the wheel's center of rotation, with clockwise defined as positive, were summed resulting in Eq. 31 through Eq. 33.

$$+\uparrow \sum F_Z: \bar{N}_R - m_R \bar{g} - F_{P,Z_R} = 0 \quad \text{Eq. 31}$$

$$+\rightarrow \sum F_{X_R}: \bar{F}_f - \bar{F}_{P,X_R} = m_R \bar{a}_{C_g,R} \quad \text{Eq. 32}$$

$$+\cup \sum M_{COR}: \tau - \bar{F}_f r = I_R \alpha_R \quad \text{Eq. 33}$$

The process was repeated for the robot platform, with the forces shown in Figure 13 decomposed into those shown in Figure 14 with moment arms defined in Figure 15.

Platform

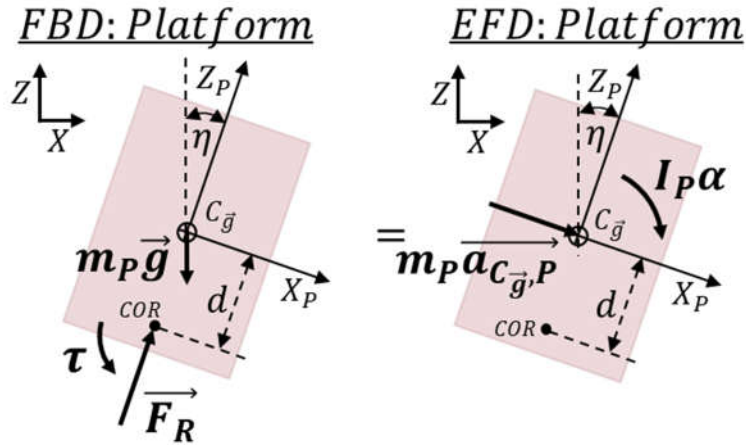


Figure 13: Free Body Diagram and Effective Force Diagram of the Robot Platform

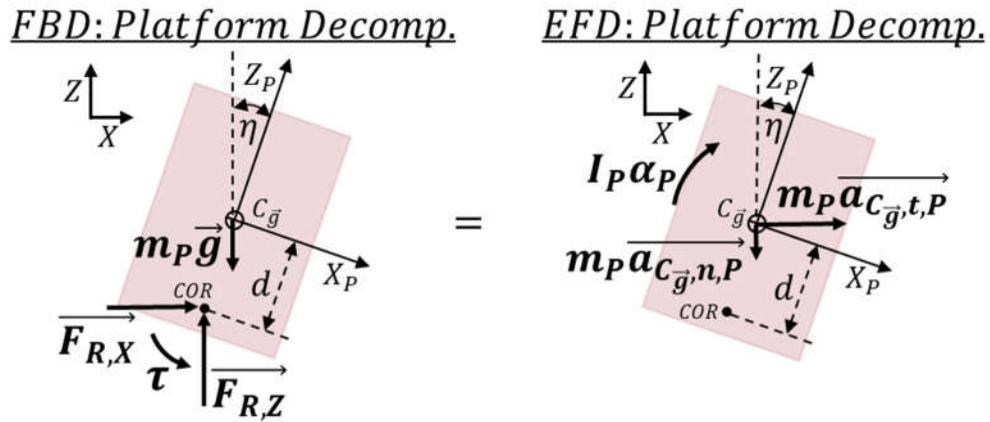


Figure 14: Free Body Diagram and Effective Force Diagram of the Platform Showing Force Components

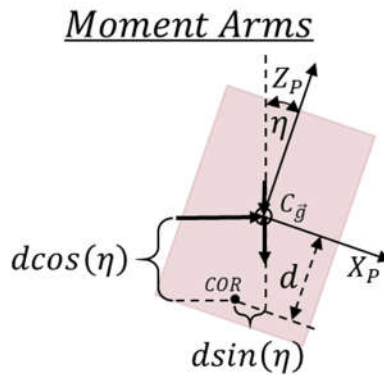


Figure 15: Diagram of Moment Arms of Forces Acting on the Platform

The sum of the forces and moments resulted in Eq. 34 through Eq. 36.

$$+\rightarrow \sum F_X: F_{R,X_P} = m_P \overrightarrow{a_{C_{\bar{g}},t,P}} \quad \text{Eq. 34}$$

$$+\uparrow \sum F_Z: F_{R,Z_P} - m_P \vec{g} = -m_P \overrightarrow{a_{C_{\bar{g}},n,P}} \quad \text{Eq. 35}$$

$$+\cup \sum M_{COR}: m_P \vec{g} d \sin(\eta) - \tau = I_P \alpha_P + m_P \overrightarrow{a_{C_{\bar{g}},t,P}} d \cos(\eta) + m_P \overrightarrow{a_{C_{\bar{g}},n,P}} d \sin(\eta) \quad \text{Eq. 36}$$

Dynamic Equations

The relationship between angular acceleration, linear acceleration, and position established in [14], and shown in Eq. 6 (from Figure 2) and Figure 11 were used to define:

$$\overrightarrow{a_{C_{\bar{g}},R}} = \ddot{x}_R = r \dot{\gamma} \quad \text{Eq. 37}$$

$$\alpha_R = \ddot{\gamma} \quad \text{Eq. 38}$$

$$\overrightarrow{a_{C_{\bar{g}},t,P}} = \ddot{x}_{C_{\bar{g}},P} \quad \text{Eq. 39}$$

$$\overrightarrow{a_{C_{\bar{g}},n,P}} = \ddot{z}_{C_{\bar{g}},P} \quad \text{Eq. 40}$$

$$\alpha_P = \ddot{\eta} \quad \text{Eq. 41}$$

The center of gravity of the platform ($C_{\bar{g}}$ in Figure 11) relative to the robot's reference frame was defined as $(X_{C_{\bar{g}},P}, Z_{C_{\bar{g}},P})$ so the acceleration of the center of gravity was defined as.

$$x_{C_{\bar{g}},P} = x_R - d \sin(\eta) \quad \text{Eq. 42}$$

$$z_{C_{\bar{g}},P} = d \cos(\eta) \quad \text{Eq. 43}$$

The derivative of the position, Eq. 42 and Eq. 43, is in the velocity of $C_{\bar{g}}$ shown in Eq. 44 and Eq. 45 and the derivative of Eq. 44 and Eq. 45 is the desired acceleration of $C_{\bar{g}}$ (Eq. 46 and Eq. 47).

$$\dot{x}_{C_{\bar{g}},P} = \dot{x}_R - d \dot{\eta} \cos(\eta) \quad \text{Eq. 44}$$

$$\dot{z}_{C_{\bar{g}},P} = -d \dot{\eta} \sin(\eta). \quad \text{Eq. 45}$$

$$\ddot{x}_{C_{\bar{g}},P} = \ddot{x}_R - d \ddot{\eta} \cos(\eta) + d \dot{\eta}^2 \sin(\eta) \quad \text{Eq. 46}$$

$$\ddot{z}_{C_{\bar{g}},P} = -d \ddot{\eta} \sin(\eta) - d \dot{\eta}^2 \cos(\eta). \quad \text{Eq. 47}$$

Eq. 35 was then solved for F_{R,Z_P} and substituted into Eq. 31 to find that

$$N_R = \vec{g}(m_R + m_P) + m_P \overrightarrow{a_{C_{\bar{g}},n,P}} \quad \text{Eq. 48}$$

Which demonstrated that the robot base supported the pendulum as expected.

The first equation of motion was developed by substituting Eq. 37 into Eq. 46 and the result into Eq. 39 to define Eq. 49. Eq. 47 was substituted into Eq. 40 to define Eq. 50.

$$\overrightarrow{a_{C_{\bar{g}},t,P}} = r\ddot{\gamma} - d\ddot{\eta} \cos(\eta) + d\dot{\eta}^2 \sin(\eta) \quad \text{Eq. 49}$$

$$\overrightarrow{a_{C_{\bar{g}},n,P}} = -d\ddot{\eta} \sin(\eta) - d\dot{\eta}^2 \cos(\eta) \quad \text{Eq. 50}$$

Eq. 49 and Eq. 50 were substituted into Eq. 36 and simplified to form the first equation of motion:

$$m_P \vec{g} d \sin(\eta) - \tau = m_P r \cos(\eta) \ddot{\gamma} - (I_P + m_P d) \ddot{\eta} \quad \text{Eq. 51}$$

The second equation of motion was developed by solving Eq. 32 for $\overrightarrow{F_f}$

$$\overrightarrow{F_f} = m_R r \ddot{\gamma} + \overrightarrow{F_{P,X_R}} \quad \text{Eq. 52}$$

and substituting the result, Eq. 52, into Eq. 33 to show

$$\tau = (I_R + r m_R) \ddot{\gamma} + F_{P,X_R} \quad \text{Eq. 53}$$

Then Eq. 49 was substituted into Eq. 34 to define F_{R,X_P} , since it is equal to F_{P,X_R} ,

$$F_{R,X_P} = m_P r \ddot{\gamma} - m_P d \ddot{\eta} \cos(\eta) + m_P d \dot{\eta}^2 \sin(\eta) \quad \text{Eq. 54}$$

The result was substituted into Eq. 53 and simplified to form the second equation of motion:

$$(I_R + r(m_R + m_P r)) \ddot{\gamma} - m_P r d \ddot{\eta} \cos(\eta) = \tau - m_P r d \dot{\eta}^2 \sin(\eta) \quad \text{Eq. 55}$$

Transfer Function and Matrix Equations

A transfer equation models the effect of one input on one output. As described balance should be achieved by controlling the motor torque to reduce the angle from vertical. Therefore, an equation that models the effect of changing the torque on the angle is necessary.

The dynamic equations found were nonlinear second order differential equations, to make finding the transfer equation easier, Eq. 51 and Eq. 55 were simplified using the small angle approximations,

$$\sin(\eta) \approx \eta \quad \text{Eq. 56}$$

$$\cos(\eta) \approx 1 \quad \text{Eq. 57}$$

Since a stable platform requires the angle from vertical be minimized as much as possible. Eq. 55 can be further simplified by recognizing that after applying the small angle approximations the change in velocity of $C_{\vec{g}}$ is sufficiently small that

$$\dot{\eta} \approx 0. \quad \text{Eq. 58}$$

The linearized balancing equations where

$$m_p \vec{g} d \eta - \tau = m_p r \ddot{\gamma} - (I_p + m_p d) \ddot{\eta} \quad \text{Eq. 59}$$

$$\tau = (I_R + r(m_R + m_p r)) \ddot{\gamma} - m_p r d \ddot{\eta}. \quad \text{Eq. 60}$$

To simplify development of the transfer equations further Eq. 59 and Eq. 60 where rewritten using the Laplace Transformation since they are still second order differential equations.

The Laplace Transform for a differential equation is

$$\mathcal{L}[f^n(t)] = s^n F(s) - s^{n-1} f(0) - s^{n-2} f'(0) \dots - s f^{n-2}(0) - f^{n-1}(0) \quad \text{Eq. 61}$$

The Laplace transformation of the differential terms in Eq. 59 and Eq. 60 where

$$\mathcal{L}[\eta(t)] = H(s) \quad \text{Eq. 62}$$

$$\mathcal{L}[\ddot{\eta}] = s^2 H(s) - s \eta(0) - \dot{\eta}(0) \quad \text{Eq. 63}$$

$$\mathcal{L}[\ddot{\gamma}] = s^2 \Gamma(s) - s \gamma(0) - \dot{\gamma}(0) \quad \text{Eq. 64}$$

The initial conditions defined in Eq. 65 where selected to investigate how chosen geometric parameters affect the robot's ability to balance.

$$\eta(0) = \gamma(0) = \dot{\eta}(0) = \dot{\gamma}(0) = 0 \quad \text{Eq. 65}$$

Eq. 59 and Eq. 60 were rewritten as Eq. 66 and Eq. 67.

$$m_p \vec{g} d H(s) - \tau = m_p r s^2 \Gamma(s) - (I_p + m_p d) s^2 H(s) \quad \text{Eq. 66}$$

$$\tau = (I_R + r(m_R + m_p r)) s^2 \Gamma(s) - m_p r d s^2 H(s). \quad \text{Eq. 67}$$

To define the transfer equation, Eq. 67 was solved for the Laplace transform of $\ddot{\gamma}$ ($\Gamma(s)$)

$$\Gamma(s) = \frac{m_p r d s^2 H(s) + \tau}{(I_R + r(m_R + m_p r))s^2} \quad \text{Eq. 68}$$

then plugged into Eq. 66 to form the transfer equation from torque to the platform's angle from vertical. The coefficients defined by Eq. 69 through Eq. 73 were used to simplify equation representation and reduce the chance for arithmetic errors.

$$q_1 = I_R + r(m_R + m_p r) \quad \text{Eq. 69}$$

$$q_2 = m_p r d \quad \text{Eq. 70}$$

$$q_3 = I_p + m_p d \quad \text{Eq. 71}$$

$$q_4 = m_p \vec{g} d \quad \text{Eq. 72}$$

$$q_5 = m_p r \quad \text{Eq. 73}$$

So the first transfer equation was determined to be

$$\frac{H(s)}{\tau} = \frac{q_1 + q_5}{q_1 q_3 s^2 + q_1 q_4 - q_2 q_5}. \quad \text{Eq. 74}$$

Since balancing may result in a change in position, the effect of the torque required to balance on the angle of the wheels was also defined to calculate the change in position. Eq. 67 was solved for $H(s)$

$$H(s) = \frac{\Gamma(s)(I_R + r(m_R + r m_p)) - \tau}{s^2 m_p r d} \quad \text{Eq. 75}$$

and substituted Eq. 75 into Eq. 66, again using the simplifying coefficients outlined in Eq. 69 through Eq. 73. The transfer equation between torque and the wheel angle was determined to be

$$\frac{\Gamma(s)}{\tau} = \frac{(q_3 - q_2)s^2 - q_4}{q_2 q_5 s^4 - q_1 q_3 s^2 - q_1 q_4}. \quad \text{Eq. 76}$$

Since Eq. 76 represents the effect of torque on the wheel angle, the change in position is defined by integrating it twice. The result can be used to adjust the global position equation

$$\xi_G = R^{-1}(\theta)\xi_R = \begin{bmatrix} \cos \theta & -\sin \theta & 0 \\ \sin \theta & \cos \theta & 0 \\ 0 & 0 & 1 \end{bmatrix} \begin{bmatrix} \frac{r}{2}(\gamma_1 + \gamma_2) \\ 0 \\ \frac{r}{2l}(\gamma_1 - \gamma_2) \end{bmatrix} \quad \text{Eq. 77}$$

by adding or subtracting the change in position to $x = \frac{r}{2}(\gamma_1 + \gamma_2)$.

4. Model Analysis

Eq. 19, which defines the robot's motion relative to the global reference frame, requires a global environment for analysis and testing which is beyond the scope of this thesis. However, the transfer equations, Eq. 74 and Eq. 76, were tested using a step and impulse response in Matlab to establish their viability as a mathematical model.

Testing Mathematical Model in Matlab

To evaluate the transfer functions initial values were selected to simulate a robot that can fit in the 8cm x 20cm x 20cm space provided for a CubeSat launch and meet the 2.5kg maximum weight limit. Lunar gravity is 1.62 m/s^2 [1], the wheels moment of inertia was calculated using $I = mr^2/2$, the moment of inertia for a wheel, and the platform moment of inertia was calculated using $I = m(2d)^2/3$, the moment of inertia for a slender rod. The slender rod's formula was chosen to demonstrate the viability of the transfer functions and would need to be replaced with the formula for the actual tool mounted on the robot's base in model implementation.

Table 1: Initial Values Used to Test Eq. 74 and Eq. 76

<i>Variable</i>	<i>r</i>	<i>m_R</i>	<i>m_P</i>	<i>d</i>	<i>I_P</i>	<i>I_R</i>	\vec{g}
<i>Test 1</i>	0.08	0.5	1	0.15	0.03	0.0016	1.62 m/s^2

The code outlined in Appendix B makes use of the simplifying coefficients listed in Eq. 69 through Eq. 73, and defines both Eq. 74 and Eq. 76 as coefficient vectors before applying Matlab's transfer function and plotting the response. Once a viable equation was established a few variances of the initial values, listed in Appendix A, were tried to establish their effect on the plot of the equation's responses to step and impulse input.

Simulation Results

Eq. 78 and Eq. 79 are the result of Matlab's transfer function for the selected values.

$$\frac{H}{\tau} = \frac{0.128}{0.00864s^2 + 0.0107} \quad \text{Eq. 78}$$

$$\frac{\Gamma}{\tau} = \frac{0.168s^2 - 0.243}{0.00096s^4 - 0.00864s^2 - 0.01166} \quad \text{Eq. 79}$$

Figure 16 and Figure 17 represent the step and impulse response for Eq. 74 and Eq. 76 respectively. The high amplitude shown in Figure 16 indicates infinite oscillation due to insufficient damping in the system. Further test results are included in Appendix C.

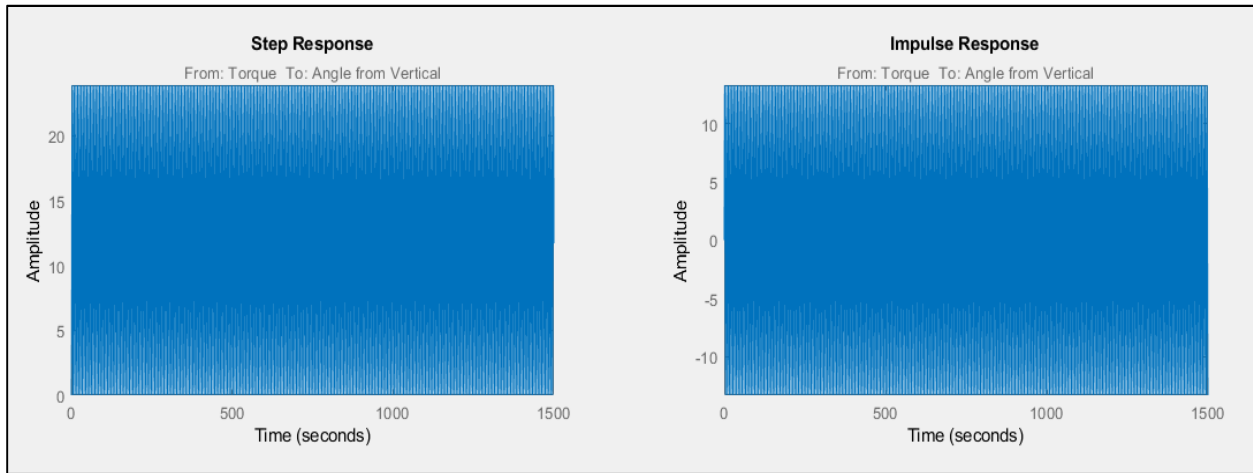


Figure 16: Step and Impulse of the Angle from Vertical to Motor Torque (Eq. 74)

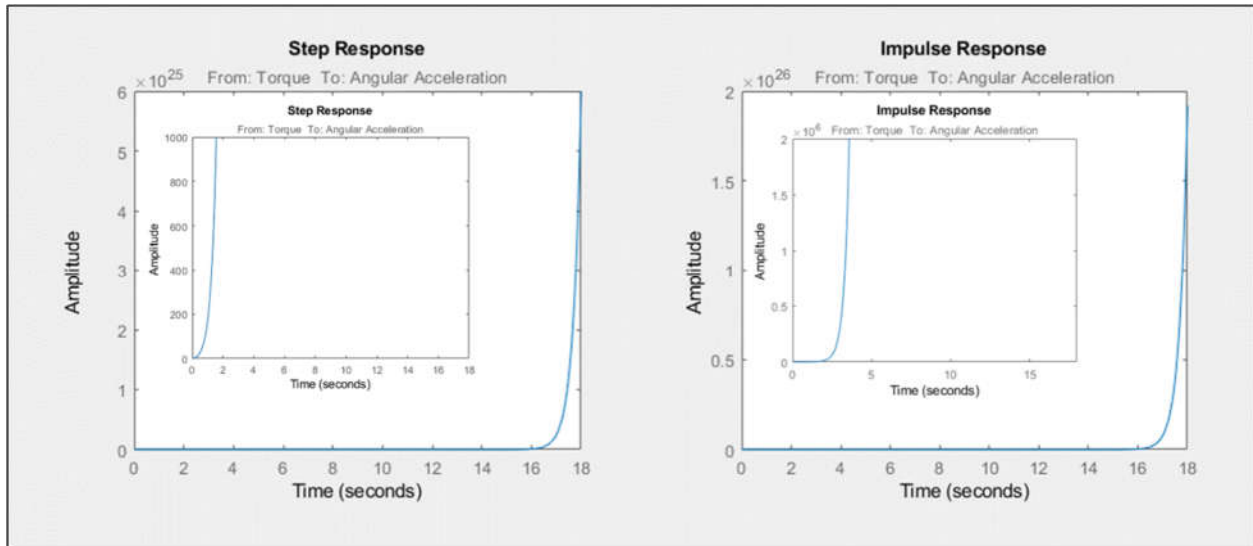


Figure 17: Step and Impulse Response of Wheel Angular Acceleration to Motor Torque (Eq. 76)

Error Analysis

The step and impulse responses demonstrated in Figure 16 and Figure 17 indicate that the mathematical model of motion is viable but that there is insufficient damping to stabilize the system.

5. Conclusions & Future Work

Conclusions

While full testing has not yet been performed, the mathematical model developed in this thesis hold up to preliminary analysis. The initial step to development of a fully autonomous two wheeled robot capable of function in a lunar environment has been successfully taken.

Future Work

This thesis laid an acceptable groundwork for future development, however the control development, and design, and testing are left for future endeavors. This means that further work can be done on the controls equations, control implementation, component selection and evaluation, physical design, and finally construction.

Controls Development and Implementation

The control method selection and controller development must still be completed. Further revising of Eq. 74 and Eq. 76 to sufficiently damp the system is required before the transfer functions developed in this thesis can be implemented. Eq. 71 should be integrated twice to the change in position due to torque required to balance and applied to Eq. 19. In addition, a minimizing function should be developed to determine the best geometry to minimize the torque required to balance the platform.

Physical testing will require writing the control software for the robot. Implemented within ROS is strongly recommended since so much of the basic framework for software development has already been completed. Additionally, implementation in ROS will allow for fully autonomous function along with the manual control required for testing the controls. This will also allow testing of Eq. 19 in ROS's native 3D simulation environment once a full CAD model has been completed.

Physical Design and Construction

While a concept for the physical design of the robot has been arrived at along with outer maximum dimensions and weight, the actual design has not been done. Components should be selected with lunar survivability and long term performance in mind to better meet the design requirements. Sensor selection must also be carried out and the physical design should incorporate those as well as mounting methods and thermal shielding where necessary. Power supply may be the most challenging for such a small robot, since enough power must be collected and stored to prevent failure during the 328 hour lunar nights.

Once the design phase has been completed, the components must be obtained or fabricated and assembled. It is likely that during this phase changes to the physical design will be required as physical implementation usually provides insights into better design practices. This means that it is likely several prototypes will need to be constructed with physical testing of each to further fine tune the design for improved function and control. Finally, the robot performance should be tested under a variety of tools to fine tune controls and define its applicability to the various jobs likely to be required in the lunar environment.

6. References

- [1] NASA, "Moon Fact Sheet," NASA, [Online]. Available: <https://nssdc.gsfc.nasa.gov/planetary/factsheet/moonfact.html>. [Accessed 15 January 2020].
- [2] J.-P. Williams, D. A. Paige, B. T. Greenhagen and E. Sefton-Nash, "The global surface temperatures of the Moon as measured by the Diviner Lunar Radiometer Experiment," *Icarus*, vol. 283, no. Lunar Reconnaissance Orbiter - Part II, pp. 300-325, 2017.
- [3] B. Dunbar, "Moon's South Pole in NASA's Landing Sites," NASA, 15 April 2019. [Online]. Available: <https://www.nasa.gov/feature/moon-s-south-pole-in-nasa-s-landing-sites>. [Accessed 23 January 2020].
- [4] Y. Zhou and Z. Wang, "Robust motion control of a two-wheeled inverted pendulum with an input delay based on optimal integral sliding mode manifold," *Nonlinear Dynamics*, vol. 85, no. 3, pp. 2065-2074, 2016.
- [5] N. Esmaili, A. Alfi and H. Khosravi, "Balancing and Trajectory Tracking of Two-Wheeled Mobile Robot Using Backstepping Sliding Mode Control: Design and Experiments," *Journal of Intelligent & Robotic Systems; Dordrecht*, vol. 87, no. 3-4, pp. 601-613, September 2017.
- [6] M. Onkol and C. Kasnakoglu, "Modeling and Control of a Robot Arm on a Two Wheeled Moving Platform," *Applied Mechanics and Materials*, Vols. 789-790, pp. 735-741, September 2015.
- [7] C. Kasnakoglu and M. Onkol, "Adaptive Model Predictive Control of a Two-wheeled Robot Manipulator with Varying Mass," *Measurement and Control*, vol. 51, no. 1-2, pp. 38-56, 16 March 2018.
- [8] C.-F. Juang, . M.-G. Lai and W.-T. Zeng, "Evolutionary Fuzzy Control and Navigation for Two Wheeled Robots Cooperatively Carrying an Object in Unknown Environments," *IEEE Transactions on Cybernetics*, vol. 45, no. 9, pp. 1731-1743, September 2015.
- [9] M. M. Rahman, Ashik-E-Rasul, H. Nowab. Md. Aminul , M. Hassan, I. M. a. Hasib and K. M. R. Hassan, "Development of a two wheeled self balancing robot with speech recognition and navigation algorithm," in *International Conference on Mechanical Engineering*, BUET, Dhaka, 2016.
- [10] M. Stillman, J. Olson and W. Gloss, "Golem Krang: Dynamically stable humanoid robot for mobile manipulation," in *IEEE International Conference on Robotics and Automation (ICRA)*, Anchorage, AK, USA , 2010.
- [11] H. W. Jones, "The Recent Large Reduction in Space Launch Cost," in *48th International Conference on Environmental Systems*, Albuquerque, New Mexico, 2018.
- [12] "Getting to Space Dosen't have to be Complicated," Spaceflight Industries, 2019. [Online]. Available: <https://spaceflight.com/schedule-pricing/#pricing>. [Accessed 2 February 2020].

- [13] R. Siegwart and I. R. Nourbakhsh, Introduction to Autonomous Mobile Robots, Cambridge, Massachusetts: The MIT Press, 2004.
- [14] R. C. Hibbeler, Engineering Mechanics Dynamics, 12th ed., Upper Saddle River, New Jersey: Pearson Prentice Hall, 2010.
- [15] E. Weisstein, "Moore-Penrose Matrix Inverse.," Mathworld--A Wolfram Web Resource, [Online]. Available: <http://mathworld.wolfram.com/Moore-PenroseMatrixInverse.html>. [Accessed 23 February 2020].
- [16] S. Ostovari, N. Morozovsky and T. Bewley, "UCSanDiego, UCSD Coordinated Robotics Lab," [Online]. Available: <http://renaissance.ucsd.edu/courses/mae143c/MIPdynamics.pdf>. [Accessed 2 April 2020].

7. Appendix

Appendix A: Values Tested

Table 2: Table of Test Values

Variable	Test 1	Test 2	Test 3	Test 4	Test 5	Test 6	Test 7
r	0.08	0.07	0.06	0.05	0.04	0.03	0.02
m_R	0.5	0.5	0.4	0.4	0.3	0.3	0.2
m_P	1	0.9	0.8	0.7	0.6	0.5	0.4
d	0.15	0.14	0.13	0.12	0.11	0.1	0.09
I_P	0.03	0.02352	0.018027	0.01344	0.00968	0.006667	0.00432
I_R	0.0016	0.001225	0.00072	0.0005	0.00024	0.000135	0.00004
\vec{g}	1.62 m/s ²						

Appendix B: Matlab Code

```
% Maximum Dimensions .08m x .2m x .2m
```

```
% Maximum Weight 2.5kg
```

```
r = 8/100; %Radius of the wheel (m)
```

```
mR = .5; %Mass of wheels (kg)
```

```
mP = 1; %Mass of Platform (kg)
```

```
d = .15; %Vertical distance from COR to platform's COG (m)
```

```
g = 9.8; %Gravity (m/s^2)
```

```
IR = (mR*r^2)/2; %Moment of Inertia of the Wheels (kg m^2)
```



```
IP = mP*(2*d)^2/3 %Moment of Inertia of a Slender Rod (kg m^2)
```

```
%Simplifying variables
```

```
q1 = IR+r*(mR+mP*r);
```

```
q2 = mP*r*d;
```

```
q3 = IP+mP*d;
```

```
q4 = mP*g*d;
```

```
q5 = mP*r;
```

```
%Transfer Function from torque to the platform angle from vertical
```

```
AfV = [q1*q3 0 q1*q4-q5*q2];
```

```
tor1 = [0 0 q1+q5];
```

```
%Transfer Function from torque to the robot's wheel's angular acceleration
```

```
AA = [q2*q5 0 -q3*q1 0 -q4*q1];
```

```
tor2 = [0 0 q3-q2 0 -q4];
```

```
sys1 = tf(tor1, AfV)
```

```
sys2 = tf(tor2, AA)
```

```
set(sys1, 'InputName','Torque')
```

```
set(sys1, 'OutputName','Angle from Vertical')
```

```
subplot(2,2,1)
```

```
step(sys1)
```

```
subplot(2,2,2)
```

```
impulse(sys1)
```

```
set(sys2, 'InputName','Torque')
```

```
set(sys2, 'OutputName','Angular Acceleration')
```

```
subplot(2,2,3)
```

```
step(sys2)
```

```
subplot(2,2,4)
```

```
impulse(sys2)
```

Appendix C: Transfer Function Output:

Test 1 Results

$$\text{sys1} = \frac{0.128}{0.00864 s^2 + 0.0107} \quad \text{Eq. 80}$$

$$\text{sys2} = \frac{0.168 s^2 - 0.243}{0.00096 s^4 - 0.00864 s^2 - 0.01166} \quad \text{Eq. 81}$$

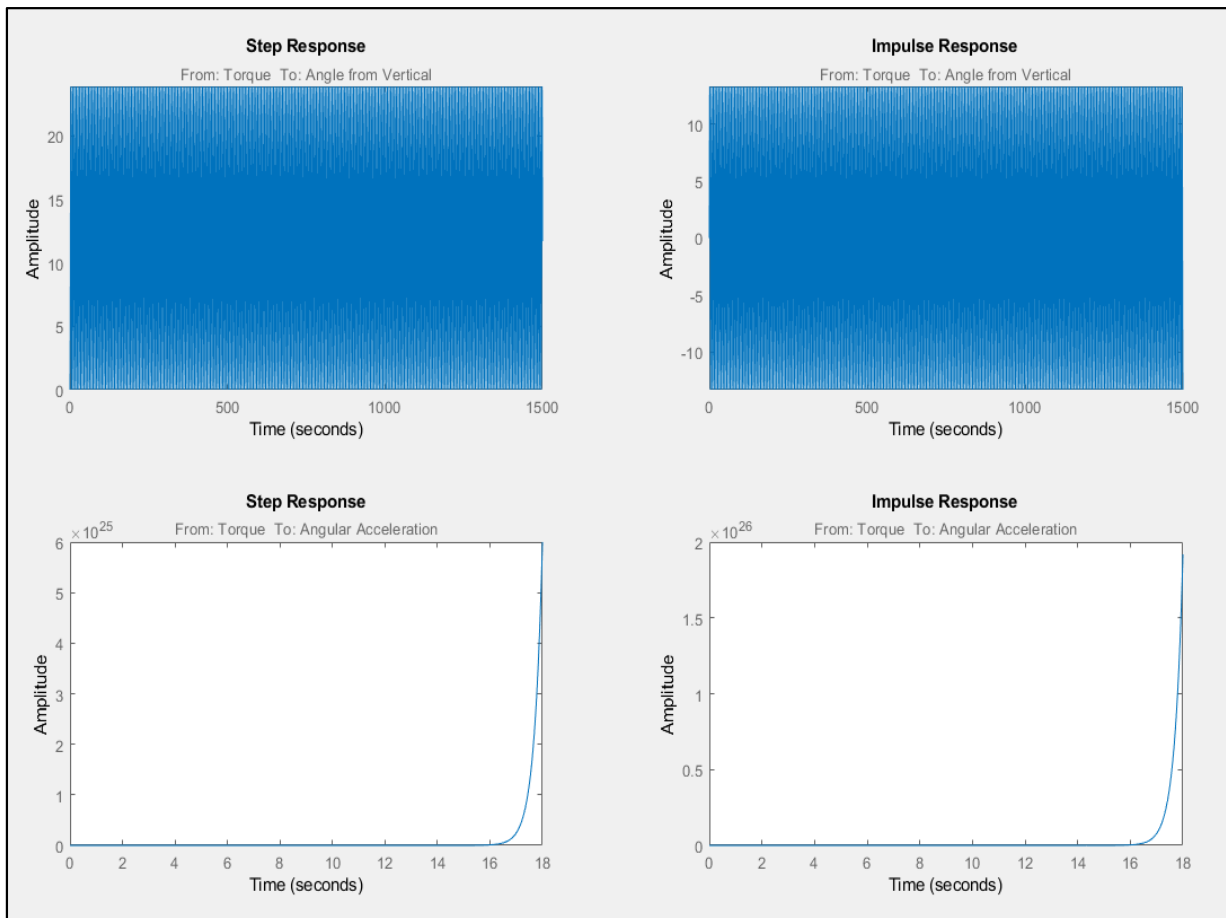


Figure 18: Test 1 Step and Impulse Response

Test 2 Results

$$\text{sys1} = \frac{0.1036}{0.006076 s^2 + 0.007739} \quad \text{Eq. 82}$$

$$\text{sys2} = \frac{0.1407 s^2 - 0.2041}{0.0005557 s^4 - 0.006076 s^2 - 0.008294} \quad \text{Eq. 83}$$

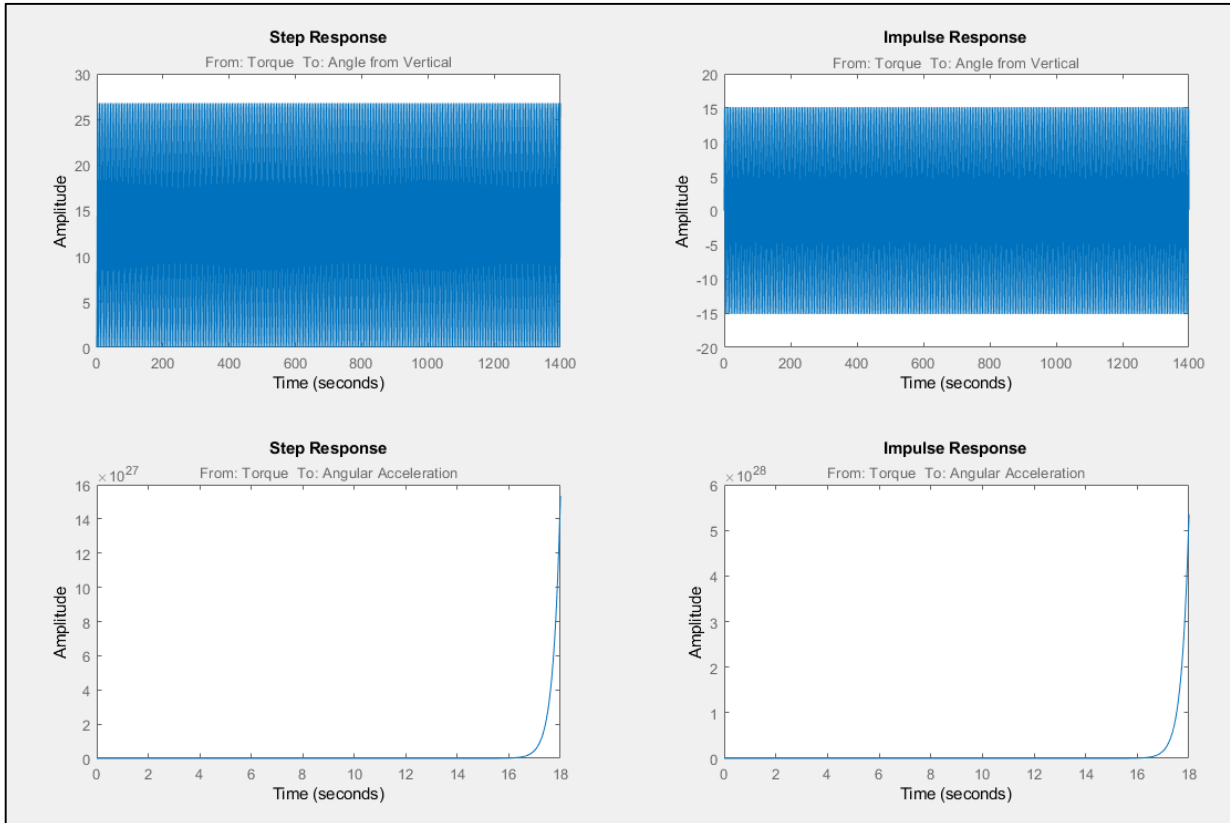


Figure 19: Test 2 Step and Impulse Response

Test 3 Results

$$\text{sys1} = \frac{0.0756}{0.003368 s^2 + 0.004351} \quad \text{Eq. 84}$$

$$\text{sys2} = \frac{0.1158 s^2 - 0.1685}{0.0002995 s^4 - 0.003368 s^2 - 0.00465} \quad \text{Eq. 85}$$

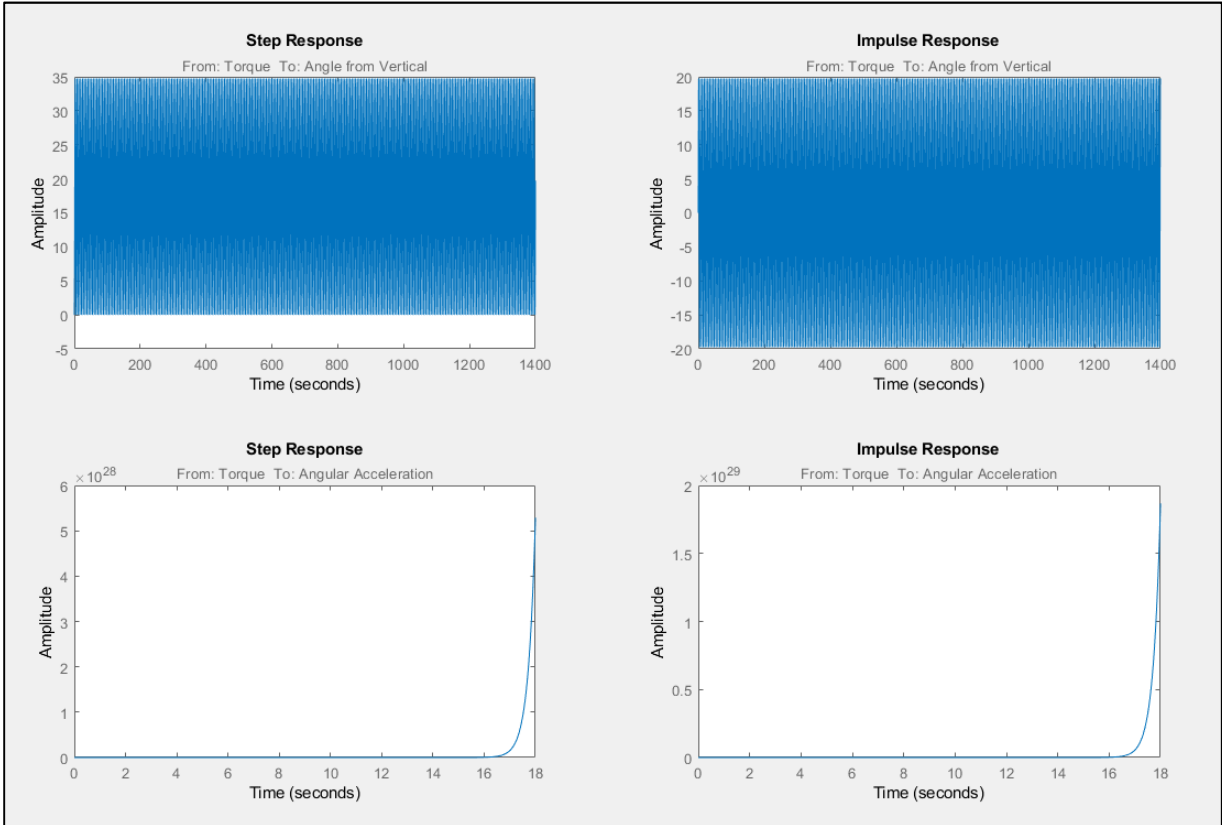


Figure 20: Test 3 Step and Impulse Response

Test 4 Results

$$\text{sys1} = \frac{0.05725}{0.002168 s^2 + 0.002881} \quad \text{Eq. 86}$$

$$\text{sys2} = \frac{0.09324 s^2 - 0.1361}{0.000147 s^4 - 0.002168 s^2 - 0.003028} \quad \text{Eq. 87}$$

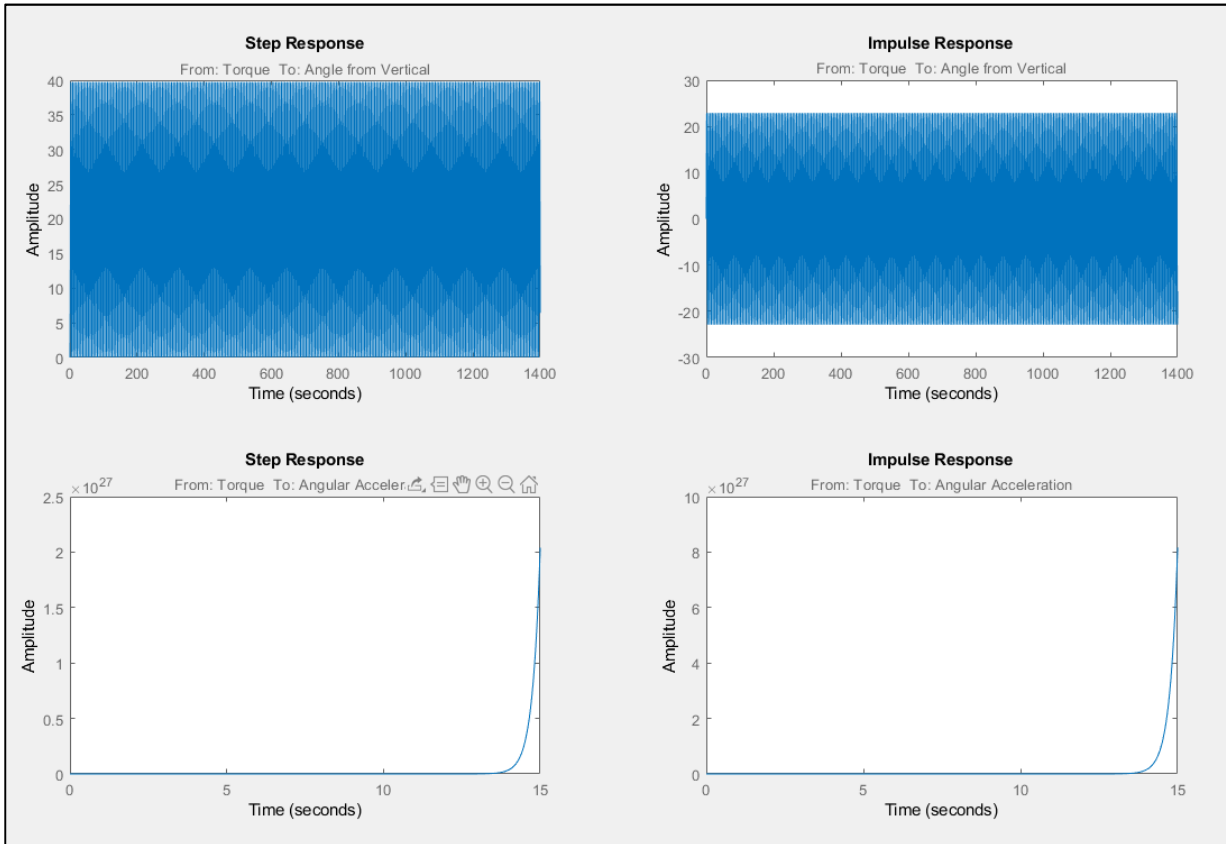


Figure 21: Test 4 Step and Impulse Response

Test 5 Results

$$\text{sys1} = \frac{0.0372}{0.000999 s^2 + 0.001348} \quad \text{Eq. 88}$$

$$\text{sys2} = \frac{0.07304 s^2 - 0.1069}{6.336e - 05 s^4 - 0.000999 s^2 - 0.001411} \quad \text{Eq. 89}$$

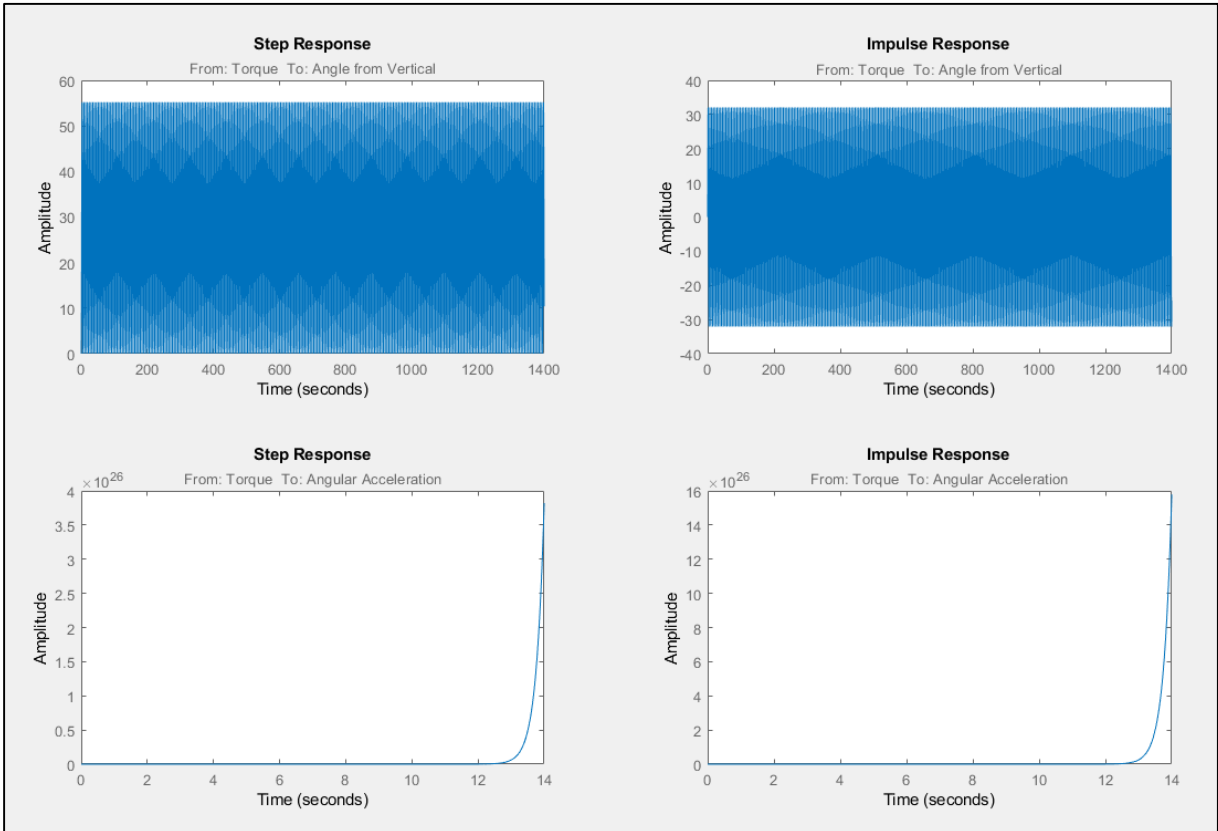


Figure 22: Test 5 Step and Impulse Response

Test 6 Results

$$\text{sys1} = \frac{0.02458}{0.0005432 s^2 + 0.0007539} \quad \text{Eq. 90}$$

$$\text{sys2} = \frac{0.05517 s^2 - 0.081}{2.25e - 05 s^4 - 0.0005432 s^2 - 0.0007764} \quad \text{Eq. 91}$$

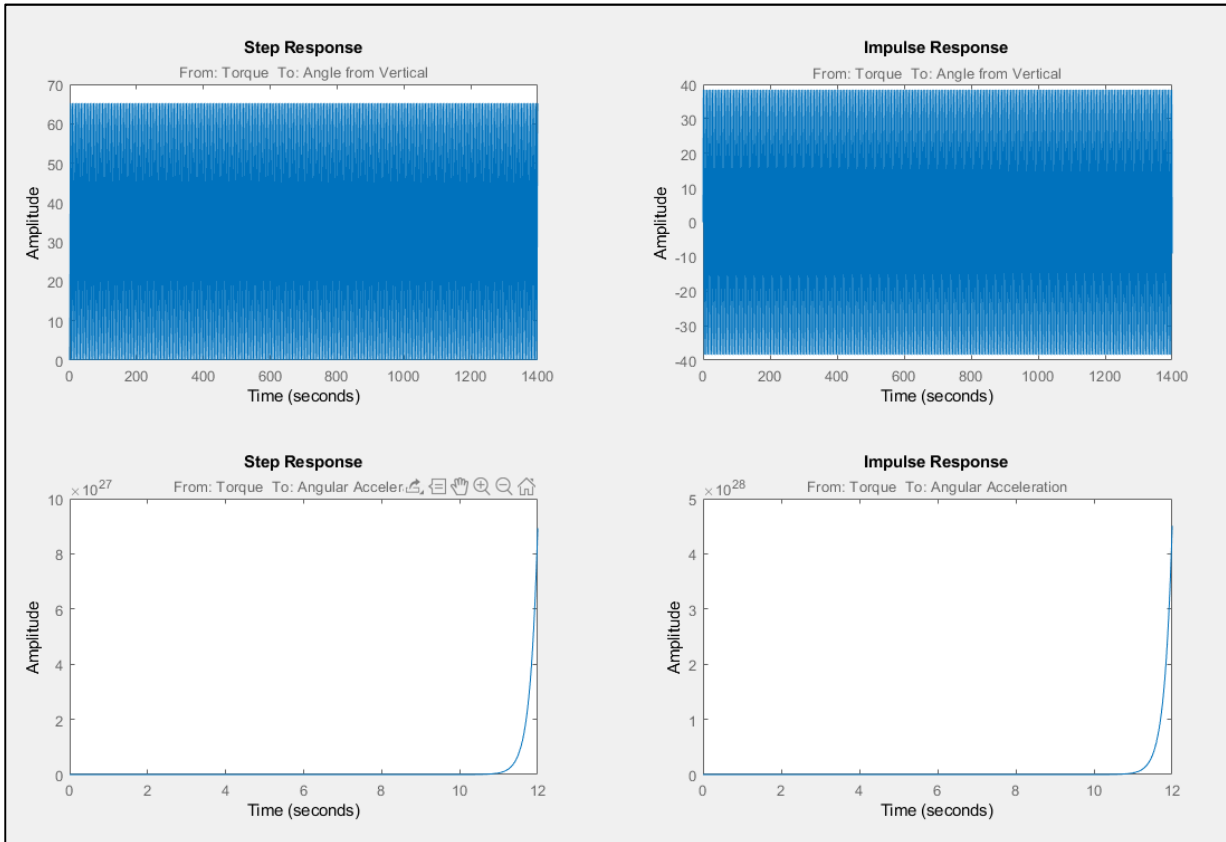


Figure 23: Test 6 Step and Impulse Response

Test 7 Results

$$\text{sys1} = \frac{0.0122}{0.0001693 s^2 + 0.0002392} \quad \text{Eq. 92}$$

$$\text{sys2} = \frac{0.0396 s^2 - 0.05832}{5.76e - 06 s^4 - 0.0001693 s^2 - 0.0002449} \quad \text{Eq. 93}$$

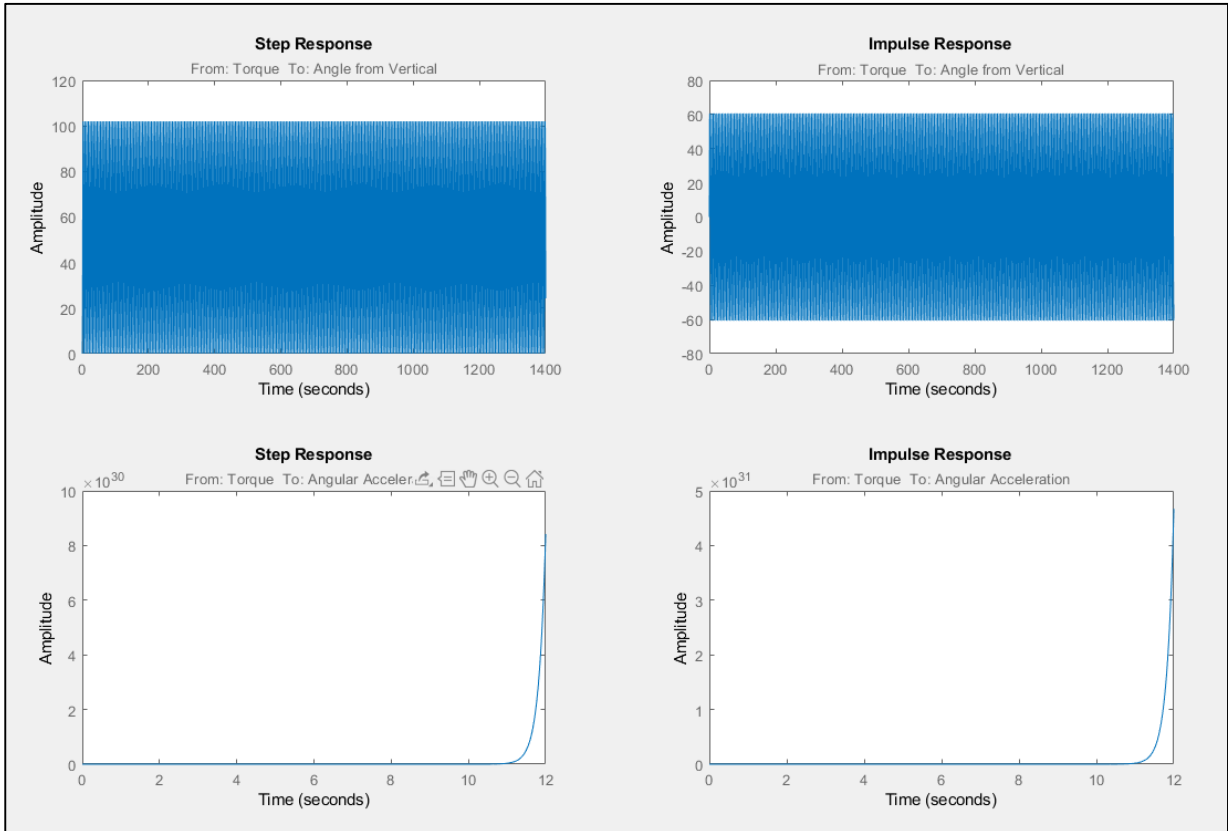


Figure 24: Test 7 Step and Impulse Response